

Spin-orbit coupling and the topology of gases of spin-degenerate cold excitons in photoexcited GaAs-AlGaAs quantum wells

M. Matuszewski,¹ T. C. H. Liew,^{2,3} Y. G. Rubo,² and A. V. Kavokin^{4,5}

¹*Instytut Fizyki Polskiej Akademii Nauk, Aleja Lotników 32/46, PL-02-668 Warsaw, Poland*

²*Centro de Investigación en Energía, Universidad Nacional Autónoma de México, Temixco, Morelos, 62580, Mexico*

³*Mediterranean Institute of Fundamental Physics, 31, via Appia Nuova, 00040, Rome, Italy*

⁴*School of Physics and Astronomy, University of Southampton, Southampton, SO17 1BJ, United Kingdom*

⁵*Spin Optics Laboratory, St-Petersburg State University, 1, Ulianovskaya, St-Petersburg, Russia*

(Received 5 April 2012; revised manuscript received 20 July 2012; published 13 September 2012)

We calculate the spatial structure of four-component spinor systems of mixed bright and dark exciton condensates in coupled quantum wells. The spin-dependent bright-dark exciton conversion and Dresselhaus spin-orbit coupling is found to generate a rich variety of topological elements. By propagating the Gross-Pitaevskii equation in imaginary time, we observe the following: single and multiple polarized vortices; the phase separation of bright and dark excitons; and exotic spatial structures in density and spin polarization.

DOI: [10.1103/PhysRevB.86.115321](https://doi.org/10.1103/PhysRevB.86.115321)

PACS number(s): 78.67.De, 03.75.Hh, 73.22.Lp, 78.55.Cr

I. INTRODUCTION

Spin-orbit coupling (SOC) is at the origin of a number of fundamental effects in solid-state physics. It is crucial for the understanding of electric-dipole spin resonances,¹ is of key importance for spintronics and quantum computation,^{2,3} and plays a central role in the physics of topological insulators,⁴ where it governs the symmetry of the ground state and induces a gap in the energy spectrum. Here, we show that SOC is also of key importance for the topology of condensates of bosons with spinor (multicomponent) order parameter.

Bosonic condensates with a spinor order parameter attracted great interest of the scientific community during the last decade. This is due to several recent experimental observations of complex spin-dependent topologies in exciton-polariton condensates in microcavities^{5,6} and in the condensates of indirect excitons in coupled semiconductor quantum wells.^{7,8} Spin patterns were predicted also for the case of synthetic spin-orbit coupling in atomic condensates.^{9,10}

Here, we focus on the excitonic system. The lowest-energy exciton states in zinc-blende semiconductor quantum wells are formed by a conduction-band electron with spin projection $+1/2$ or $-1/2$ on the structure axis and a heavy hole, the quasispin projections on the structure axis of which are $+3/2$ or $-3/2$. Consequently, the exciton spin projections are $+2$, -2 , $+1$, or -1 . The $+2$ and -2 exciton states are decoupled from light. These are so-called “dark excitons.” Contrarily, the $+1$ and -1 excitons may be strongly coupled to light and they form bright exciton-polariton states in semiconductor microcavities. This is why condensates of exciton polaritons have a two-component order parameter, describing the amplitudes and phases of exciton polaritons with spin projections $+1$ and -1 . Here, we study theoretically the topological properties of condensates of spatially indirect excitons in biased coupled quantum wells GaAs/AlGaAs. In these systems, bright excitons weakly interact with light due to the low overlap integral of electrons and holes, which is why exciton condensates remain nearly or fully fourfold degenerate.

We investigate the topological properties of such four-component exciton condensates in the presence of SOC terms linear in the wave vector. Two such terms can appear due to

the lack of inversion symmetry in zinc-blende semiconductor quantum wells in the presence of an electric field: the Dresselhaus term^{11,12} and the Rashba term.^{13,14} The effects of both terms are qualitatively similar, but we will be mainly interested in the Dresselhaus terms for electrons and holes, which are shown to play an important role in recent experiments on cold exciton gases.¹⁵ We also include the effect of the trapping potential, which was recently used for establishing full coherence of the condensate.⁸ We show that competition of spin-orbit coupling, trapping, and interactions can induce the emergence of various spin structures, including vortices, vortex arrays, or spin domains. We also demonstrate that the competition of electron- and hole-induced couplings leads to a peculiar hidden asymmetry in the Hamiltonian, which breaks the symmetry of dark and bright exciton states.

II. GROSS-PITAEVSKII EQUATIONS

We describe a Bose-Einstein condensate in a quasi-two-dimensional geometry, where the exciton gas is effectively trapped in the (x, y) plane, with a four-component order parameter $\Psi = (\psi_{+2}, \psi_{+1}, \psi_{-1}, \psi_{-2})^T$, where $\psi_{\sigma}(\mathbf{r}_{\perp}, t)$ with $\sigma = \pm 2$ and ± 1 are the dark and the bright exciton components, respectively. The mean-field Hamiltonian density of the system is

$$\mathcal{H} = \Psi^{\dagger} \cdot \mathbf{H}^{(1)} \cdot \Psi + \frac{1}{2} V_0 n^2 + W(\psi_{+2}^* \psi_{-2}^* \psi_{+1} \psi_{-1} + \text{c.c.}), \quad (1)$$

where $n = \sum_{\sigma} |\psi_{\sigma}|^2$ is the total density and

$$\mathbf{H}^{(1)} = \left[\frac{\hbar^2 \mathbf{k}^2}{2M} + U(\mathbf{r}_{\perp}) \right] \mathbf{I} + \mathbf{H}_{\text{so}}, \quad (2)$$

$$\mathbf{H}_{\text{so}} = \begin{pmatrix} 0 & \beta_e \hat{k}_+ & \beta_h \hat{k}_- & 0 \\ \beta_e \hat{k}_- & 0 & 0 & \beta_h \hat{k}_- \\ \beta_h \hat{k}_+ & 0 & 0 & \beta_e \hat{k}_+ \\ 0 & \beta_h \hat{k}_+ & \beta_e \hat{k}_- & 0 \end{pmatrix}, \quad (3)$$

with $\hat{\mathbf{k}} = -i\nabla$ and $\hat{k}_{\pm} = \hat{k}_x \pm \hat{k}_y$.

The above Hamiltonian includes the Dresselhaus coupling for electrons (β_e) and holes (β_h), the spin-independent dipole-dipole repulsion of excitons described by the coefficient V_0 , spin-dependent bright-dark exciton scattering described by the coefficient W , and the external harmonic potential $U(\mathbf{r}_\perp) = M\omega^2 \mathbf{r}_\perp^2/2$. In principle, there are also weak spin-dependent exciton-exciton interactions due to the spin dependence of the exchange.¹⁶ For simplicity, we neglect them since they do not lead to qualitative changes in the exciton condensate topology. On the other hand, taking into account the mixing W term is crucial since it describes the scattering of two bright excitons into two dark ones (and the reverse process) and leads to a coupling of phases of the different components.

The Gross-Pitaevskii equations generated by the Hamiltonian density, defined by Eqs. (1)–(3), are

$$i\hbar \frac{\partial \psi_{\pm 2}}{\partial t} = \frac{\hbar^2 \hat{\mathbf{k}}^2}{2M} \psi_{\pm 2} + \beta_e \hat{k}_\pm \psi_{\pm 1} + \beta_h \hat{k}_\mp \psi_{\mp 1} + U(\mathbf{r}_\perp) \psi_{\pm 2} + V_0 n \psi_{\pm 2} + W \psi_{\mp 2}^* \psi_{\mp 1} \psi_{\mp 1}, \quad (4a)$$

$$i\hbar \frac{\partial \psi_{\pm 1}}{\partial t} = \frac{\hbar^2 \hat{\mathbf{k}}^2}{2M} \psi_{\pm 1} + \beta_e \hat{k}_\mp \psi_{\pm 2} + \beta_h \hat{k}_\mp \psi_{\mp 2} + U(\mathbf{r}_\perp) \psi_{\pm 1} + V_0 n \psi_{\pm 1} + W \psi_{\mp 1}^* \psi_{\pm 2} \psi_{\mp 2}. \quad (4b)$$

III. WEAK POTENTIAL TRAP

We have performed the numerical minimization of the energy of the system with the imaginary-time method. Results for the case of a weak potential trap are shown in Fig. 1, for different values of W .

At high exciton densities, the ground-state profile depends on the sign of W . For negative W , the system tends to form a plane wave in each component as shown in Fig. 1(a), while for positive W , the phase-separated stripe state is preferred, as in Fig. 1(b). These states are not a special feature of the trapped system, but also appear in a planar system. They can be understood by considering single-particle ground states in a homogeneous system.¹⁰ The Hamiltonian in the absence of interactions is $H_0 = \hbar^2 \mathbf{k}^2/2M + H_{\text{so}}$ and due to the presence of linear in \mathbf{k} SOC terms, the single-particle energy is minimized at the finite wave vector $|\mathbf{q}| = M|\beta_e + \beta_h|/\hbar^2$. This solution corresponds to the plane wave

$$\begin{pmatrix} \psi_{+2} \\ \psi_{+1} \\ \psi_{-1} \\ \psi_{-2} \end{pmatrix} = e^{i\mathbf{q}\cdot\mathbf{r}} \sqrt{\frac{n}{4}} \begin{pmatrix} 1 \\ e^{i\varphi_{\mathbf{q}}} \\ e^{-i\varphi_{\mathbf{q}}} \\ 1 \end{pmatrix}, \quad (5)$$

where $\varphi_{\mathbf{q}} = \arg(q_x + iq_y)$. In the presence of interactions, the system chooses to form either a single plane wave or a superposition of two antiparallel plane waves, depending on the sign of spin-dependent interactions W . The solution (5) minimizes the exciton mixing energy for negative W , which leads to the condensate in a single plane-wave state with all components mixed [Fig. 1(a)]. On the other hand, for positive W , there is frustration of plane-wave solutions (5) since to minimize the exciton mixing energy one needs to change the sign of one of the components. This frustration leads to phase separation of dark and bright

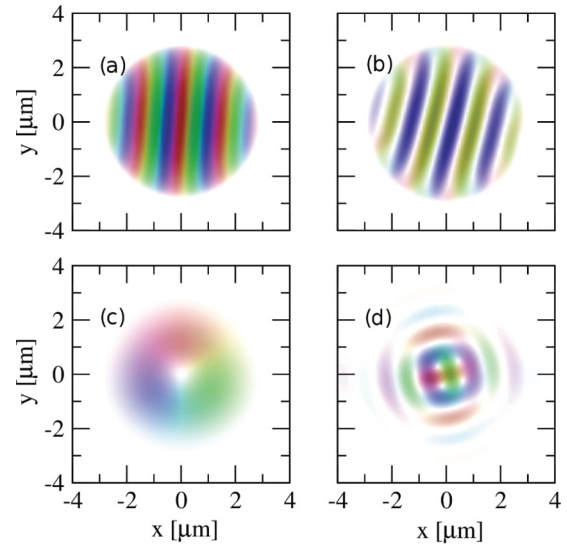


FIG. 1. (Color online) Examples of ground states of the system (only the ψ_{+1} component is shown). The darker regions correspond to higher exciton density, and the colors depict the phase of the wave function. In the case of strong interactions and spin-orbit coupling, (a) plane-wave solutions exist for $W < 0$ and (b) spin-domain (stripe) solutions exist for $W > 0$. If interactions are weak compared to the trapping energy scale, (c) single-vortex or (d) multiple-vortex solutions are present in the cases of weak and strong spin-orbit coupling, respectively. The parameters are $n = 10^{10} \text{ cm}^{-2}$, $\beta_e = 10 \text{ meV \AA}$ except (c), $\beta_e = 2 \text{ meV \AA}$ in (c), $\beta_h = \beta_e/2$, $V_0 = 0.1 \mu\text{eV } \mu\text{m}^2$ in (a), (b), $V_0 = 10^{-5} \mu\text{eV } \mu\text{m}^2$ in (c), (d), $W = -0.2V_0$ in (a), $W = 0.2V_0$ in (b).

components, which is realized by the standing wave solution (see Fig. 2).

At low exciton densities, the interactions are weak, and the SOC terms become dominant. The ground-state patterns in this regime generally consist of one or many vortices, similar to the case of atomic condensates.⁹ The vortices are formed as a result of interference of several plane-wave ground states. The SOC and mixing of components imposes some restrictions on the winding numbers of vortices that can be formed in exciton condensates.

First, we note that minimization of the exciton mixing energy [last term in (1)] results in locking between the phases

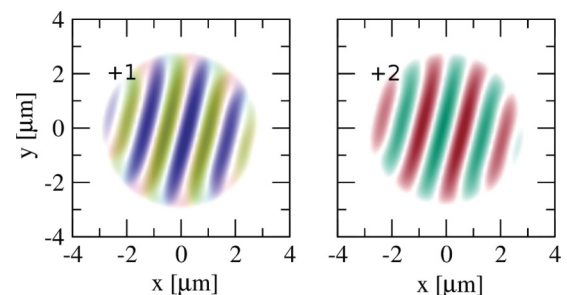


FIG. 2. (Color online) Spin structure of the spin-domain (stripe) solution from Fig. 1(b). The domains of dark and bright excitons complement each other, keeping the total density close to the Thomas-Fermi profile. The ψ_{-1} and ψ_{-2} components are identical to their positive counterparts.

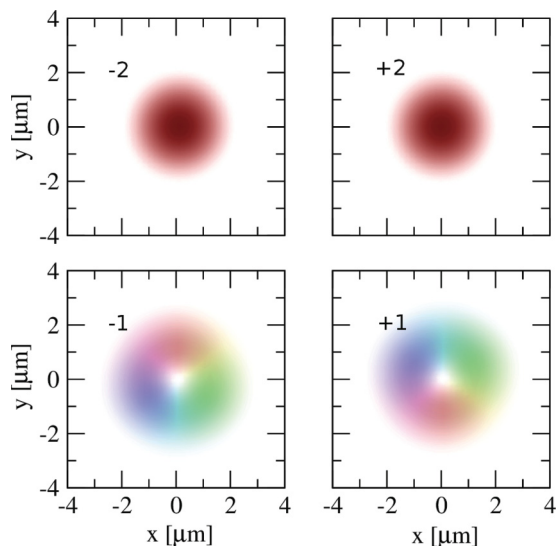


FIG. 3. (Color online) The single vortex ground state from Fig. 1(c). The vorticity in the spin components follows the rule (7) imposed by the spin-orbit coupling.

of different components. If one writes $\psi_\sigma = \sqrt{n_\sigma} \exp\{i\theta_\sigma\}$, then the phases should satisfy $\theta_{+2} + \theta_{-2} - \theta_{+1} - \theta_{-1} = 0$ or $\pi \pmod{2\pi}$ for $W < 0$ and $W > 0$, respectively. This condition should hold far away from the vortex core, and it bounds the winding numbers m_σ of different components to obey

$$m_{+2} + m_{-2} = m_{+1} + m_{-1}. \quad (6)$$

The second bound is due to SOC and it appears for the cylindrically symmetric solutions of Eqs. (4a) and (4b), i.e., for vortices with $\theta_\sigma = -\mu t + m_\sigma \phi$, where μ is the chemical potential and ϕ is the azimuthal angle in the quantum well plane. It is easy to see that since $\hat{k}_\pm \exp\{im_\sigma \phi\}$ transforms like $\exp\{i(m_\sigma \pm 1)\phi\}$, one has

$$m_{+2} = m_{+1} + 1 = m_{-1} - 1 = m_{-2} \quad (7)$$

for these vortices. The conditions (6) and (7) are consistent with each other, but while the bound (6) is strict, the bound (7) applies only to the vortices with cylindrical symmetry. There can be warped vortex solutions of Eqs. (4a) and (4b) obeying (6), but not satisfying (7), similar to the warped vortices in two-component condensates with two branches of single-particle energy.¹⁷

The broken symmetry of dark and bright exciton states, evident in Fig. 3, is a consequence of the bound rule (7), but is not straightforwardly apparent in the Hamiltonian of the system. The simplest vortex solution of this type has opposite vorticities in $\psi_{\pm 1}$, while winding numbers are zero in the $\psi_{\pm 2}$ components, forming a generic $(0, -1, +1, 0)$ spin vortex. This asymmetry is found in all solutions which contain vortices, but is absent in solutions in which radial symmetry is not present, such as the plane-wave or spin-domain states.

We summarize the results of more systematic calculations of ground states in a diagram in Fig. 4. Here, the strength of the spin-orbit coupling and system size was kept constant, while the spin-dependent and spin-independent interaction

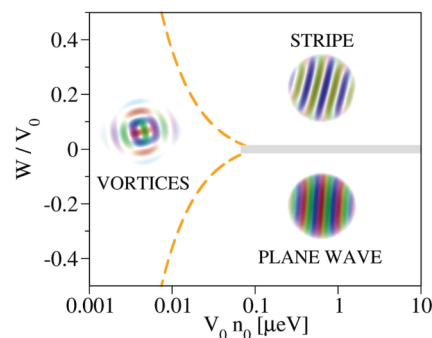


FIG. 4. (Color online) Showing the crossovers between different ground states of the system with fixed spin-orbit coupling coefficients $\beta_e = 10 \text{ meV \AA}$ and $\beta_h = 5 \text{ meV \AA}$ and varying interaction coefficients V_0 and W . The size of the trap was adjusted to keep the size of the condensate similar to that of Fig. 1–3. The number of vortices in the phase on the left depends on the system size. Shaded region around $W = 0$ indicates the domain where the mean-field approximation is not reliable.

coefficients W and V_0 were varied. In the regime of small interaction strength, the ground state is in general composed of spin vortices described above, independently of the sign of W . In the strong interaction regime, the sign of W determines the ground state of the system, which is the “stripe” state for positive W and “plane wave” for negative W .

It should be noted that the validity of mean-field approximation used in this study is limited by high enough values of

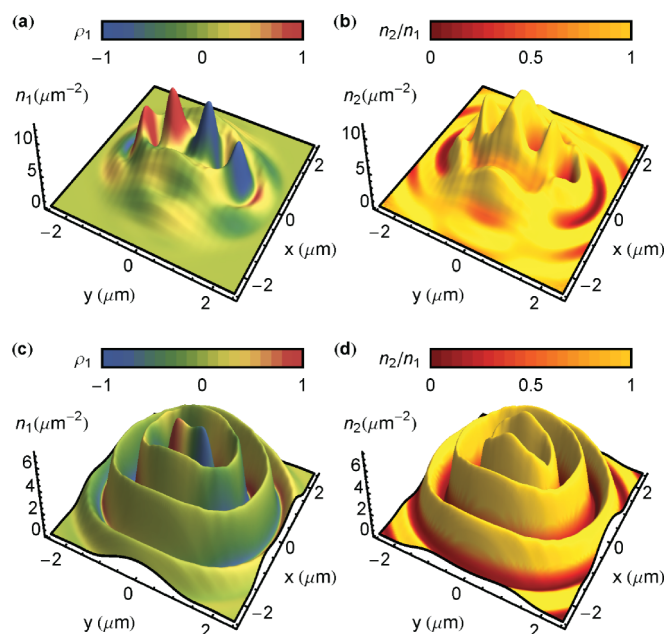


FIG. 5. (Color online) Spatial structure of four-component condensates in a strong potential trap ($m_{\text{ex}}\omega/2 = 1 \mu\text{eV}\mu^{-2}$). The bright (a) and dark (b) exciton intensity is shown for the case $W = -0.2V_0$. The variation of the spin-polarization degree of bright excitons is shown by the colors in (a). Dark excitons have approximately zero circular polarization degree. The ratio of the dark to bright exciton density is shown by the colors in (b). (c) and (d) show the corresponding profiles for the case $W = 0.2V_0$.

the mixing parameter W , and fluctuations play an important role for $|W| \ll V_0$. Moreover, the order is expected to be destroyed for $W = 0$ as in the high-dimensional nonlinear sigma model.¹⁸ This is why the detailed behavior of crossover lines in Fig. 4 can not be established for small W (in the shaded region).

IV. STRONG POTENTIAL TRAP

In the case of a strong potential trap, the broken rotational symmetry caused by the Dresselhaus terms allows strong spin polarizations in the spatial structure of the ground states. Figures 5(a) and 5(b) show the density of bright (n_1) and dark (n_2) exciton components for $W = -0.2V_0$. The spin-polarization degree of bright excitons, $\rho_1 = (|\psi_{+1}| - |\psi_{-1}|)/(|\psi_{+1}| + |\psi_{-1}|)$, is illustrated by the colors in Fig. 5(a). Comparing the maxima of the density profiles, we observe that bright and dark components separate, similar to the behavior observed in Figs. 1 and 2. We note that indications of phase separation of dark and bright excitons in strain-induced traps were reported in Ref. 19. The minima of the density profiles correspond to the existence of vortices in the corresponding fields (not shown), in analogy to the half-vortices observed in two-component condensates with spin-orbit coupling.^{5,20} For the case $W = +0.2V_0$, the bright and dark exciton densities form a set of co-centric distorted rings. Again, a spin polarization of bright excitons can be observed in addition to phase separation of the bright and dark excitonic components in real space.

V. CONCLUSIONS

We studied four-component exciton condensates in a two-dimensional quantum well structure in the presence of Dresselhaus spin-orbit coupling. The spin-sensitive interactions introduced by the ability of pairs of bright excitons to scatter into dark excitons (and vice versa) play a crucial role in determining the spatial structure. In weak potential traps, bright and dark exciton condensates may phase separate depending on the sign of the bright-dark exciton interaction W . Single- and multiple-vortex solutions can also appear depending on the interaction strengths and the strength of Dresselhaus spin-orbit coupling terms. In the presence of a strong potential trap, the Dresselhaus terms allow separation of different spin-polarized components and the formation of nontrivial structures in both the excitonic densities and spin polarization. The selection of structures that we have studied demonstrate the intricate variety of patterns obtainable in four-component spinor systems, which are expected to persist under nonequilibrium experimental conditions.

ACKNOWLEDGMENTS

M.M. acknowledges support from the Foundation for Polish Science through the ‘‘Homing Plus’’ program. This work was supported in part by DGAPA-UNAM under the Project No. IN112310 and by the EU FP7 IRSES project POLAPHEN. AK acknowledges funding from the Russian Ministry of Science and Education. TL thanks the support of the FP7 Marie Curie project ‘‘EPOQUES’’ (298811).

¹E. I. Rashba and V. I. Sheka, in *Landau Level Spectroscopy*, edited by G. Landwehr and E. I. Rashba (North-Holland, Amsterdam, 1991), p. 131.

²I. Žutić, J. Fabian, and S. Das Sarma, *Rev. Mod. Phys.* **76**, 323 (2004).

³*Semiconductor Spintronics and Quantum Computation*, edited by D. D. Awschalom, D. Loss, and N. Samarth (Springer, Berlin, 2002).

⁴M. Z. Hasan and C. L. Kane, *Rev. Mod. Phys.* **82**, 3045 (2010).

⁵K. G. Lagoudakis, T. Ostatnický, A. V. Kavokin, Y. G. Rubo, R. André, and B. Deveaud-Plédran, *Science* **326**, 974 (2009).

⁶C. Adrados, A. Amo, T. C. H. Liew, R. Hivet, R. Houdré, E. Giacobino, A. V. Kavokin, and A. Bramati, *Phys. Rev. Lett.* **105**, 216403 (2010).

⁷A. A. High, J. R. Leonard, A. T. Hammack, M. M. Fogler, L. V. Butov, A. V. Kavokin, K. L. Campman, and A. C. Gossard, *Nature (London)* **483**, 584 (2012).

⁸A. A. High, J. R. Leonard, M. Remeika, L. V. Butov, M. Hanson, and A. C. Gossard, *Nano Lett.* **12**, 2605 (2012).

⁹Y.-J. Lin, K. Jimenez-Garcia, and I. B. Spielman, *Nature (London)* **471**, 83 (2011); S. Sinha, R. Nath, and L. Santos, *Phys. Rev. Lett.* **107**, 270401 (2011); H. Hu, B. Ramachandran, H. Pu, and X.-J. Liu, *ibid.* **108**, 010402 (2012).

¹⁰C. Wang, C. Gao, C.-M. Jian, and H. Zhai, *Phys. Rev. Lett.* **105**, 160403 (2010).

¹¹G. Dresselhaus, *Phys. Rev.* **100**, 580 (1955).

¹²M. I. D’yakonov and V. Y. Kachorovskii, *Fiz. Tekh. Poluprovodn.* **20**, 178 (1986) [*Sov. Phys.–Semicond.* **20**, 110 (1986)].

¹³E. I. Rashba, *Fiz. Tverd. Tela (Leningrad)* **2**, 1224 (1960) [*Sov. Phys.–Solid State* **2**, 1109 (1960)].

¹⁴Yu. A. Bychkov and E. I. Rashba, *Pisma Zh. Eksp. Teor. Fiz.* **39**, 66 (1984) [*JETP Lett.* **39**, 78 (1984)].

¹⁵J. R. Leonard, Y. Y. Kuznetsova, Sen Yang, L. V. Butov, T. Ostatnický, A. Kavokin, and A. C. Gossard, *Nano Lett.* **9**, 4204 (2009).

¹⁶Y. G. Rubo and A. V. Kavokin, *Phys. Rev. B* **84**, 045309 (2011).

¹⁷M. Toledo Solano and Y. G. Rubo, *Phys. Rev. B* **82**, 127301 (2010).

¹⁸A. Pelissetto and E. Vicari, *Phys. Rep.* **368**, 549 (2002).

¹⁹N. W. Sinclair, J. K. Wuenschell, Z. Vörös, B. Nelsen, D. W. Snoke, M. H. Szymańska, A. Chin, J. Keeling, L. N. Pfeiffer, and K. W. West, *Phys. Rev. B* **83**, 245304 (2011).

²⁰B. Ramachandran, B. Opanchuk, X.-J. Liu, H. Pu, P. D. Drummond, and H. Hu, *Phys. Rev. A* **85**, 023606 (2012).